

This work was written as part of one of the author's official duties as an Employee of the United States Government and is therefore a work of the United States Government. In accordance with 17 U.S.C. 105, no copyright protection is available for such works under U.S. Law.

Public Domain Mark 1.0

<https://creativecommons.org/publicdomain/mark/1.0/>

Access to this work was provided by the University of Maryland, Baltimore County (UMBC) ScholarWorks@UMBC digital repository on the Maryland Shared Open Access (MD-SOAR) platform.

Please provide feedback

Please support the ScholarWorks@UMBC repository by emailing scholarworks-group@umbc.edu and telling us what having access to this work means to you and why it's important to you. Thank you.

The light (H^+ , H_2^+ , He^+) and heavy (Na^+) pickup ion dynamics in the lunar-like plasma environment: 3D hybrid kinetic modeling

A.S. Lipatov^{a,*}, J.F. Cooper^b, E.C. Sittler Jr.^b, R.E. Hartle^b

^a *GPHI UMBC/NASA GSFC, Code 673, Greenbelt, MD 20771, USA*

^b *NASA Goddard Space Flight Center, Greenbelt, MD 20771, USA*

Received 9 June 2013; received in revised form 8 August 2013; accepted 18 August 2013

Available online 29 August 2013

Abstract

In this report we discuss the self-consistent dynamics of pickup ions in the solar wind flow around the lunar-like object. In our model the solar wind and pickup ions are considered as particles, whereas the electrons are described as a fluid. Inhomogeneous photoionization, electron-impact ionization and charge exchange are included in our model. The Moon will be chosen as a basic object for our modeling. The current modeling shows that mass loading by pickup ions H^+ , H_2^+ , He^+ , and Na^+ may be very important in the global dynamics of the solar wind around the Moon. In our hybrid modeling we use exponential profiles for the exospheric components. The Moon is considered as a weakly conducting body. Special attention will be paid to comparing the modeling pickup ion velocity distribution with ARTEMIS observations. Our modeling shows an asymmetry of the Mach cone due to mass loading, the upstream flow density distribution and the magnetic field. The pickup ions form an asymmetrical plasma tails that may disturb the lunar plasma wake. © 2013 COSPAR. Published by Elsevier Ltd. All rights reserved.

Keywords: Exospheres; Pickup ions; Induced magnetospheres; Satellites; Plasma modeling

1. Introduction

The hybrid kinetic model used here supports comprehensive modeling of the interaction between different spatial and energetic elements of the Moon-solar wind-magnetosphere of the Earth system. This involves variable upstream magnetic field and solar wind plasma, including energetic ions, electrons, and neutral atoms. This capability is critical to improved interpretation of existing measurements for surface and exospheric composition from previous missions and planning future missions.

Lunar observations show the existence of several species of the neutrals and pickup ions like Na , He , K , O etc., (see

e.g., Tyler et al., 1988; Potter and Morgan, 1988; Tanaka et al., 2009; Hartle and Killen, 2006). Hartle and Killen (2006) have provided the measurable lower limits of exosphere densities with currently known upper limits inside exosphere: $n_{Na} = 17 - 70 \text{ cm}^{-3}$, $n_{He} = 336 - 2000 \text{ cm}^{-3}$, $n_O = 321 - 500 \text{ cm}^{-3}$, $n_H = 65 - 17 \text{ cm}^{-3}$, and $n_{H_2} = 7.6 - 9000 \text{ cm}^{-3}$. Recently, MAP-PAGE-IMA (Plasma energy Angle and Composition Experiment, and Ion Mass Analyzer) onboard Japanese lunar orbiter SELENE (KAGUYA) detected Moon originating ions at 100 km altitude. Ion species of H^+ , He^{++} , He^+ , C^+ , O^+ , Na^+ , K^+ , and Ar^+ were definitively identified. The Solar Wind Ion Detectors (SWIDs) on the Chang'E-1 spacecraft, while orbiting the Moon, occasionally observed two continuous flux peaks with energies not exceeding 8 and 4 times that of the prevailing solar wind energy (Wang et al., 2011b).

There is a set of MHD (Wolf, 1968; Spreiter et al., 1970), kinetic (Birch and Chapman, 2001), hybrid (Kallio, 2005; Travnicek et al., 2005; Lipatov and Cooper, 2010; Wang

* Corresponding author. Tel.: +1 3012860906; fax: +1 3012861648.

E-mail addresses: Alexander.Lipatov-1@nasa.gov, alipatov@umbc.edu (A.S. Lipatov), John.F.Cooper@nasa.gov (J.F. Cooper), Edward.C.-Sittler@nasa.gov (E.C. Sittler Jr.), Richard.E.Hartle@nasa.gov (R.E. Hartle).

¹ Address: Moscow Institute of Physics and Technology, Russia.

et al., 2011a; Holmström et al., 2012; Wiehle et al., 2011), drift kinetic (Whang, 1969; Whang and Ness, 1970; Catto, 1974; Lipatov, 1976; Lipatov, 2002; Lipatov et al., 2005), and electrostatic (Farrell et al., 1998; Tao et al., 2012), and Monte Carlo (Lee et al., 2011) modeling of the lunar plasma environment.

Wave-particle interactions play a very important role in plasma dynamics near the Moon: mass loading, excitation of low-frequency waves and the formation of the non-Maxwellian particle velocity distribution function. Particle-wave interactions play a very important role in the possible formation of an oblique shock wave system inside the lunar plasma wake, and in coupling of pickup ions and the upstream ions via excitation of low-frequency waves. These kinetic processes become important in the formation of an obstacle for the upstream flow.

Magnetohydrodynamic (MHD) models have been useful for the study of the interaction between plasma flow and the Moon (Wolf, 1968; Spreiter et al., 1970). MHD modeling demonstrated a global picture of magnetospheric interaction with the Moon, formation of the plasma wake with external rarefaction waves and oblique shock structures. However, several kinetic effects are not included in the MHD formalism, namely: anisotropy of the ion velocity distribution which results to excitation of the low-frequency electromagnetic waves, formation of the electron and ion beams and excitation of the high-frequency waves, etc. Many of these effects may be recovered by using hybrid or full kinetic modeling.

In papers by Whang (1969), Whang and Ness (1970), and Lipatov (1974, 1975, 1976), they had studied the structure of the lunar plasma wake in the “guiding center” approximation. These models produced the magnetic field perturbations which are in a good agreement with onboard observations of the lunar wake by the Explorer 35 spacecraft. The “guiding center-in-cell” numerical modeling (Lipatov, 1976) also produced the magnetic field perturbation in the case of nonstationary solar wind and the conducting lunar core. A quasi-MHD (Chew-Goldberger-Low) approach (Chew et al., 1956) with anisotropic pressure has also described well the electromagnetic perturbations in the lunar wake (Catto, 1974). Several 3D hybrid modeling of the Moon plasma interactions were performed during the last decade as described in papers by Kallio (2005), Travnicek et al. (2005), Lipatov et al. (2005), Lipatov and Cooper (2010), Wang et al. (2011a), and Holmström et al. (2012). These models describe well wave-particle interactions, in particular, the anisotropy of the ion velocity distributions. The hybrid models demonstrate the formation of the oblique shock-like structure in the middle of the lunar wake. The hybrid modeling by Wiehle et al. (2011) has been devoted to an interpretation of the ARTEMIS data and good agreement was produced.

The hybrid kinetic model allows us to take into account the finite gyroradius effects of pickup ions and to correctly estimate the ion velocity distribution and the fluxes along the magnetic field, and on the lunar surface. Modeling

shows the formation of the asymmetric Mach cone, the structuring of the pickup ion tails, and presents another type of lunar-solar wind interaction. We will compare the results of our modeling with observed distributions.

In our study the model of the neutral exosphere (H , H_2 , He , Na) are chosen from Hartle and Killen (2006). Note, that we already performed the modeling the dynamics of O^+ and (Na^+ , He^+) pickup ions near the Moon (Lipatov et al., 2011b; Lipatov et al., 2012a). The solar wind parameters are chosen from the ARTEMIS observations (Wiehle et al., 2011). We apply a time-dependent Boltzmann’s “particle-in-cell” approach (Lipatov et al., 1998), together with a hybrid plasma (ion kinetic) model (Lipatov et al., 2002b) in three spatial dimensions (see, e.g. Lipatov and Combi, 2006) using a prescribed but adjustable neutral exosphere and the heavy ion clouds model for the Moon. A Boltzmann modeling is applied to model charge exchange between (incoming and pickup) ions and the immobile exospheric neutrals. In this paper we discuss the results of hybrid kinetic modeling of the lunar environment, namely, global plasma structures, e.g., the formation of the asymmetrical Mach cone, magnetic barrier, pickup ion tails etc. The results of this kinetic modeling are compared with the ARTEMIS flyby observational data. Comparison of results of our hybrid model with other ARTEMIS flybys (Halekas et al., 2011) will be presented in a future publication.

The paper is organized as follows: in Section 2 we present the computational model and a formulation of the problem. In Section 3 we present the results of modeling the plasma environment near the Moon and comparison with observational data. Finally, in Section 4 we summarize our results and discuss the future development of our computational model.

2. Formulation of the problem and mathematical model

To study the interaction of the solar wind with the ionized and neutral components of the lunar environment we use a quasi-neutral hybrid model, namely, a kinetic description for the upstream and pickup ions, and a fluid approximation for electrons. The hybrid model accurately describes wave-particle interactions on the following ion spatial (λ) and time (ω^{-1}) scales: $\lambda \sim \rho_{ci} = U_0/\Omega_i$ or $\lambda \sim c/\omega_{pi}$ and $\lambda \gg \rho_{ce}$; $\omega \leq \Omega_i$, where ρ_{ci} and ρ_{ce} denote the gyroradii for ions and electrons (respectively); U_0 is the bulk velocity of the background plasma; c/ω_{pi} denotes the ion inertial length, and Ω_i is the ion gyrofrequency. The length λ may represent either the wave-length of the excited low-frequency waves or the spatial scale of the plasma structures and boundaries in the Lunar environment. The model includes photoionization, electron impact ionization and charge exchange. We explicitly include ionization, mass-loading and charge exchange as the dominant mechanisms for the interaction away from the lower boundary at the Moon. We also include finite conductivity, given by the diffusion scale length, at the inner boundary.

The exosphere is considered to be an immobile component in this paper.

The general scheme of the global interaction of the solar wind with the Moon and the ARTEMIS trajectory is given in Fig. 1. The ARTEMIS flybys always occurred behind the Moon. The orbit does not directly cross the center of the wake. In our coordinate system the X axis is directed away from the Sun, Y is directed in the direction of Earth's orbit, and Z axis completes the right-handed system.

In the hybrid model described here, the dynamics of upstream ions and implanted ions use a kinetic approach, while the dynamics of the electrons is described by a hydrodynamical approximation. We use a standard 3D hybrid code (see e.g. Lipatov et al., 2011b; Lipatov, 2002 for details). Here we assume that the mass and charge state of the ions are M_s and $Z_s = 1$. The subscript s denotes the ion population: $s = 1$ for H^+ upstream ions and $s = 2, 3, 4, 5$ for H^+ , H_2^+ , He^+ , and Na^+ pickup ions. We also take into account the interaction of ions with neutral particles by charge exchange (see Eqs. 12,13,14,15 from Lipatov and Combi (2006)), and we assume that the bulk velocity and thermal temperatures of neutral particles equal zero.

We further assume quasi-neutrality

$$n_e = \sum_{s=1}^{N_{\text{species}}} n_s. \quad (1)$$

For massless electrons the equation of motion of the electron fluid takes the form of standard generalized Ohm's law (e.g. Braginskii, 1965):

$$\mathbf{E} = \frac{\mathbf{J}_e \times \mathbf{B}}{en_e c} - \frac{\nabla p_e}{en_e} \quad (2)$$

where $p_e = nm_e \langle v_e'^2 \rangle / 3 = n_e T_e$ is the scalar electron pressure, and v_e' is the thermal velocity of electrons; J_e denotes the electron current.

Since we suppose that electron heating due to collisions with ions is very small, the electron fluid is considered adiabatic. For simplicity we assume that the total electron

pressure may be represented as a sum of partial pressures of all electron populations:

$$p_e \propto \frac{(\beta_e n_{i,\text{up}}^{5/3} + \sum_s \beta_{e,\text{PI},s} n_{i,\text{PI},s}^{5/3})}{\beta_e}, \quad (3)$$

where β_e and $\beta_{e,\text{PI},s}$ denote electron beta for the upstream and pickup populations, respectively. We also assume here that $n_{e,\text{up}} = n_{i,\text{up}}$, and $n_{e,\text{PI},s} = n_{i,\text{PI},s}$. Here, $n_{i,\text{iono}}$ denotes the immobile heavy pickup ion cloud. Otherwise, we have to calculate the electron pressure from heat balance for electrons (see, e.g., Braginskii, 1965) taking into account the heat fluxes for pickup electrons and exospheric electrons on the right side of this equation. The ion kinetic approach allows us to take into account the effects of anisotropy of ion pressure, the correct mass loading processes, the penetration of ions across the exosphere, and the asymmetry of plasma flow around the Moon. Recall that the fluid models, which account only for the scalar (i.e., isotropic) ion pressure, may result in an extra-expansion of the pickup ions along the magnetic field. Our computational model may also include charge exchange between magnetospheric ions and exospheric atoms, and between heavy pickup ions and exospheric atoms (see, e.g., Lipatov and Combi, 2006).

The neutral exosphere of the Moon serves as a source of new ions, mainly by electron stimulated desorption (McLain et al., 2011) and also by photoionization. The neutral exosphere also serves as collisional targets for charge exchange with the upstream flow H^+ ions. The impacting ions consist both of upstream flow ions as well as newly implanted ions which are picked up by the motional electric field.

We have adopted a four-species description for the neutral exosphere of the exponentials form

$$n_{\text{neutral},k} = \Psi(\theta, \phi) n_{\text{exo},k} \exp(-(r - r_{\text{exobase}})/h_{\text{exo},k}) \quad (4)$$

Eq. (4) represents a numerical approximation of the exosphere model for the Moon. The function $\Psi \propto \cos^2 \theta$ has a maximum value in the direction toward the Sun, and it has a zero value at the night-side. In Eq. (4), $n_{\text{exo},k}$ is the maximum value of the neutral density extrapolated to the exobase, and $r_{\text{exobase}} \approx R_M$. Index k denotes H , H_2 , He , and Na . Here the maximum value of the neutral density at the exobase are $n_{\text{exo},H} = 1.0 \times 10^2 \text{ cm}^{-3}$, $n_{\text{exo},H_2} = 3.0 \times 10^3 \text{ cm}^{-3}$, $n_{\text{exo},He} = 2.0 \times 10^3 \text{ cm}^{-3}$, and $n_{\text{exo},Na} = 1.0 \times 10^2 \text{ cm}^{-3}$ (Wang et al., 2011b). Note that these values are much less than the experimental total exospheric density of considerably larger scale height of atoms released via sputtering into the exosphere (Wurz et al., 2007). The model developed in Hartle and Thomas (1974) gives the following range for the maximum value of He density: $2 \times 10^3 \text{ cm}^{-3} < n_{\text{exo},He} < 4 \times 10^4 \text{ cm}^{-3}$. We now study the models with much low value of the neutral density at the exobase. The spatial scales are $h_{\text{exo},H} = 1990 \text{ km}$, $h_{\text{exo},H_2} = 1000 \text{ km}$, $h_{\text{exo},He} = 498 \text{ km}$, and $h_{\text{exo},Na} = 87 \text{ km}$ (Hartle and Killen,

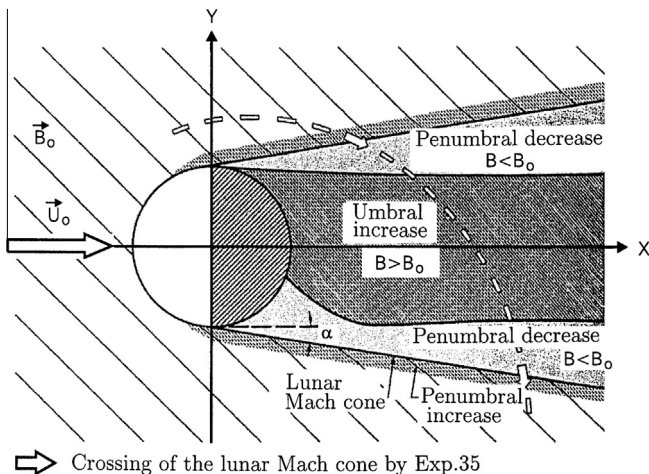


Fig. 1. Lunar plasma environment and the system of coordinates.

2006). The thermal velocity of all newly formed pickup ions is about 2.0 km/s.

The production of new ions from the exosphere near the Moon corresponds to

$$G_{\text{exo},k} = \Psi(\theta, \phi) v_{i,k} n_{\text{exo},k} \exp[(r - r_{\text{exobase}})/h_{\text{exo},k}]. \quad (5)$$

Here $n_{\text{exo},k}$ denotes the value of the neutral component density at $r = r_{\text{exobase}}$ and $v_{i,k}$ is the effective ionization rate per atom or molecule of species k . The effective value of the ionization are $v_{i,H} = 7.5 \times 10^{-7} \text{ s}^{-1}$, $v_{i,H_2} = 1.47 \times 10^{-7} \text{ s}^{-1}$, $v_{i,He} = 7.8 \times 10^{-9} \text{ s}^{-1}$ (Wang et al., 2011b), and $v_{i,Na} = 1.8 \times 10^{-5} \text{ s}^{-1}$ (Potter and Morgan, 1988; Wang et al., 2011b; Gruntman, 1996). The total pickup ion production rates are $Q_{H^+} \approx 5.0 \times 10^{21} \text{ s}^{-1}$, $Q_{H_2^+} \approx 1.0 \times 10^{22} \text{ s}^{-1}$, $Q_{He^+} \approx 1.0 \times 10^{21} \text{ s}^{-1}$, and $Q_{Na^+} \approx 2.0 \times 10^{22} \text{ s}^{-1}$.

The physical processes near the moon are described by total pickup ion production rates rather than by local values of the pickup ion production rates. The generation of pickup ions was produced with a variable weight of the macro-particles (see. e.g. Lipatov, 2012).

2.1. Initial conditions

Initially the computational domain contains only super-Alfvénic and supersonic solar wind flow with a homogeneous spatial distribution and a Maxwellian velocity distribution; the pickup ions have a weak density and spherical spatial distribution. The magnetic field and electric fields are $\mathbf{B} = \mathbf{B}_0$ and $\mathbf{E} = -\mathbf{U}_0 \times \mathbf{B}_0/c$. Inside the Moon the electromagnetic fields are $\mathbf{E} = 0$ and $\mathbf{B} = \mathbf{B}_0$, and the bulk velocities of ions and electrons also equal to zero.

At $t > 0$ we begin to inject the pickup ions with a distribution according to Eq. (5). Far upstream ($x = -5L$, where $L = R_M$), the ion flux is assumed to have a Maxwellian distribution,

$$f = n_\infty (\pi v_{th}^2)^{-3/2} \exp \left[-\frac{(\mathbf{v} - \mathbf{U})^2}{2v_{th}^2} \right], \quad (6)$$

where v_{th} and \mathbf{U} are the thermal and the bulk velocities of the background plasma flow, respectively.

2.2. Boundary conditions

At the side boundaries we use a damping boundary condition for the electromagnetic field. At the back boundary we use a “Sommerfeld” radiation condition for the magnetic field, and a free escape condition for particles, with re-entry of a portion of the particles from the outflow plasma. The magnetic field and electric fields are $\mathbf{B} = \mathbf{B}_0$ and $\mathbf{E} = -\mathbf{U}_0 \times \mathbf{B}_0/c$.

Inside the Moon, the bulk velocities of ions and electrons also equal to zero.

We also take into account the effect of the finite conductivity of the lunar body so that

$$\begin{aligned} R_{m,eff} &= R_{m,shell}, & \text{for } R_M > r > R_{core}, \\ R_{m,eff} &= R_{m,core}, & \text{for } r \leq R_{core}, \end{aligned} \quad (7)$$

where $R_{m,shell}$ and $R_{m,core}$ denote the effective magnetic Reynolds numbers ($R_m = 4\pi U_0 L \sigma_{eff}/c^2$) in the weak-conducting shell and conducting core, the values of which are presented in Sect. “Results of Modeling”. R_{core} is the radius of the lunar core. Note, that of Cartesian mesh can provide a solution of the Maxwell equations only in the first approximation. The more precise solution inside the lunar interior one has to use the spherical system of coordinates (see, e.g. Lipatov, 1976).

Far downstream, we adopted a free escape condition for particles and Sommerfeld’s radiation condition for the magnetic field. On the side boundaries ($y = \pm DY/2$ and $z = \pm DZ/2$), periodic boundary conditions were imposed for incoming flow particles and the electromagnetic field. The pickup ions exit the computational domain when they intersect the surfaces $y = \pm(DY/2 - 5 \times \Delta y)$, or $z = \pm(DZ/2 - 5 \times \Delta z)$, or $x = 20L - 5 \times \Delta x$. Thus there is no influx of pickup ions at the side boundaries. At the Lunar surface, $r = R_M$, the particles are absorbed. There is no boundary condition for the electromagnetic field, and we also use our equations for the electromagnetic field inside the Moon, but with internal conductivity and the bulk velocity that is calculated from the particles. In this way the jump in the electric field is due to the variation of the value of the conductivity and bulk velocity across the lunar surface. Note that the position of the center of the Moon is $x = 0$, $y = 0$, $z = 0$.

The three-dimensional computational domain has dimensions $DX = 25L$, $DY = 40L$, and $DZ = 20L$, where $L = R_M = 1738 \text{ km}$. We used meshes of $251 \times 401 \times 201$ grid points, and 6×10^8 and 8×10^7 macro-particles for protons and pickup ions, respectively, for a homogeneous mesh computation. The time step Δt satisfies the condition $v_{max} \Delta t \leq \min(\Delta x, \Delta y, \Delta z)/16$.

The relationship between dimensional (U, E, B, p_e, n, T) and dimensionless (U', E', B', p'_e, n', T') parameters may be expressed via the dimensional upstream values as follows:

$$\begin{aligned} \mathbf{U} &= \mathbf{U}' U_0, & \mathbf{E} &= \mathbf{E}' B_0 U_0/c, & \mathbf{B} &= \mathbf{B}' B_0, & p_e &= p_e' p_{e0}, \\ n &= n' n_0, & T &= T' M_i U_0^2, \end{aligned} \quad (8)$$

whereas the dimensional time and distance may be expressed via the bulk velocity U_0 and characteristic scale $L = R_M$:

$$t = t' L/U_0, \quad \mathbf{x} = \mathbf{x}' L. \quad (9)$$

The global physics in the lunar environment is controlled by a set of dimensionless independent parameters such as M_A , β_i , β_e , M_{PI}/M_p , ion production and charge exchange rates, diffusion lengths, and the ion gyroradius ρ_{ci} . For real values of the magnetic field the value of the H^+ upstream ion, He^+ and Na^+ pickup ion gyroradii are about 250 km, 1000 km and 5700 km (respectively) which are calculated from the local bulk velocity. The grid spacing has the value $\Delta_x = 175 \text{ km}$.

In order to study ion kinetic effects (e.g. excitation of low-frequency oscillations ($\omega \ll \Omega_b$) by the mass loading), we must satisfy the condition $\Delta \leq (10 - 20)c/\omega_{pb}$, where Ω_b and ω_{pb} denote the gyrofrequency and the plasma frequency for background ions (Winske et al., 1985). The above estimation of the plasma parameters shows that we have good resolution for the low-frequency waves. To excite high-frequency waves ($\Omega_b \ll \omega \ll \Omega_e$) we must satisfy the condition $\Delta \leq 0.25c/\omega_{pb}$, (Winske et al., 1985) for background ions. The above estimation shows that we have insufficient resolution for the high-frequency waves.

3. Results of the modeling

To study the interaction of the solar wind with the heavy ion cloud near the Moon the following sets of the magnetospheric plasma and exosphere parameters were adopted in accordance with flyby observational data: upstream velocity, densities and magnetic field: $U_0 = 305$ km/s; $\mathbf{U}/U_0 = (0.983, -0.164, -0.065)$; $n_0 = n_{H^+} = 3.0$ cm⁻³; $B_0 = 5.2$ nT; $\mathbf{B} = (-1., 1.0, 5.0)$ nT; $M_A = 5.17$; $M_S = 3.66$; $\beta_{H^+} = 0.2$; $\beta_e = 0.5$ and $\beta_{pickup,e} = 0.05$. The effective Reynolds numbers inside the shell and core of the Moon are $R_{m,shell} = 0.05$ and $R_{m,core} = 0.2$. The radius of the lunar core R_{core} equals $0.5R_M$.

In this section we discuss the results of a modeling at time $t = 5 T_{transit}$, where $T_{transit}$ denotes an average transition time for particle from the left (upstream) boundary to the right (downstream) boundary.

3.1. Global structure of the lunar environment

Figs. 2 and 3 demonstrate 2-D cuts of the (H^+ , He^+ , Na^+) pickup ion density. The x - y cuts (left column) are located at $z/L = 0$, y - z cuts (middle column) are located at $x/L = 2.4$, and x - z cuts (right column) are located at $y/L = 0$. Let us consider at first the distribution of light pickup ions. Fig. 2 shows the cuts of the distribution of the H^+ (top) and He^+ (bottom) pickup ions. Pickup ions create a halo around the moon which is transformed into the relatively thin tails oblique to the lunar plasma wake. These tails represents a complex three-dimensional inhomogeneous structures. Due to a small value of the gyroradius the light ions are “frozen in” to the background plasma flow at the short distance, $\propto \rho_{ci}$ (see e.g. Winske et al., 1985; Galeev et al., 1987). The light pickup ions play important role in the heavier pickup ion dynamics inside the halo. The light pickup ions are also effectively filling the center of the plasma wake where the background plasma has a small density.

The He^+ pickup ion density (top) and Na^+ pickup ion density (bottom) are shown in Fig. 3. The x - y cuts (left column) are located at $z/L = 0$, y - z cuts (middle column) are located at $x/L = 2.4$, and x - z cuts (right column) are located at $y/L = 0$. The modeling shows the formation of the asymmetrical Mach cone (for $y < 0$, Fig. 4, top) in the

solar wind due to mass loading by the heavy pickup ions (for $y > 0$, Fig. 3 bottom). The modeling also demonstrates three peaks in the background H^+ ion density profile across the Mach cone transition ($N_{H^+,2}/n_0 \approx 2.0; 1.5; 1.3$) for $x = 2.4 L$ and $z = 0$. The average value of the proton density inside the Mach cone is about $1.2n_0$. Note that value of peak ion densities are lower than in previous modeling without light (H^+ , He^+) pickup ions (Lipatov et al., 2012a). The ARTEMIS observations (see Figs. 4 and 5 from Wiehle et al. (2011)) also show three peaks in the density profile ($N_{H^+,2}/n_0 \approx 1.4; 1.3; 1.1$) for the time interval $09.40 \leq t \leq 09.50$ ($2.2 < x/L < 2.6$, $0 < y/L < -0.3$, and $1.4 < z/L < 1.7$). However, these peaks are wider and weaker that it were observed in our modeling. Such disagreement may be explained by the overestimated conductivity of the lunar interior model or by the possible dissipation processes. The central region of the plasma wake is oblique to the solar wind bulk velocity.

The modeling gives the following maximum values of the background and pickup ion density near the exobase: $n_{H^+,max} = 1.1 n_0$, $n_{He^+,max} = 3 \times 10^{-5} n_0$, $n_{H_2^+,max} = 7 \times 10^{-4} n_0$, $n_{He^+,max} = 1.5 \times 10^{-5} n_0$, $n_{Na^+,max} = 3 \times 10^{-4} n_0$, where $n_0 = 3.0$ cm⁻³. The Na^+ heavy pickup ions form a complex two-tail structure - external and internal tails. The external tail is formed by the pickup ions created near the lunar surface with $y > 0$. The internal tail is formed by the pickup ions created on the other side of the lunar surface. The splitting the pickup ion environment into a two-tail structure may be explained by the acceleration of pickup ions due to the polarization electric field. Near the exobase, the radial electric field is mainly determined by the electron pressure and it is oriented out of exobase. The splitting the pickup ion tail was also observed in the modeling of the solar wind-weak comet interaction (see, e.g. Lipatov et al., 1997; Lipatov, 2002). The trajectory of the heavy Na^+ pickup ions in the outer tail is similar to a test particle motion with an average value of the gyroradius about of 3×10^4 km. The heavy He^+ pickup ions also create two-tail structure. The ions in outer tail move along the cycloid with average gyroradius about of 5×10^3 km. The internal tail has a quasi-straight form with perturbations along the tail. A small portion of the He^+ pickup ions move along the cycloid just between the external and internal tails.

Fig. 4 (bottom) and Fig. 5 show the 2-D cuts of the B_x , B_y and B_z magnetic field profiles. Here, the x - y cuts (left column) are located at $z/L = 0$, y - z cuts (middle column) are located at $x/L = 2.4$, and x - z cuts (right column) are located at $y/L = 0$. Figs. 4 and 5 (left and right columns, bottom) also confirms a formation of the asymmetrical Mach cone. As one may see that magnetic field topology follows the upstream H^+ profile for $y < 0$ (asymmetric Mach cone) and weak perturbation in the region of the heavy Na^+ pickup ion mass loading, Fig. 3 (bottom). The value of the magnetic field in the lobe side of the magnetic barrier is about $2.7B_0$. The average jump in the magnetic field at the front of the Mach cone is about $B_2/B_0 \approx 1.6$.

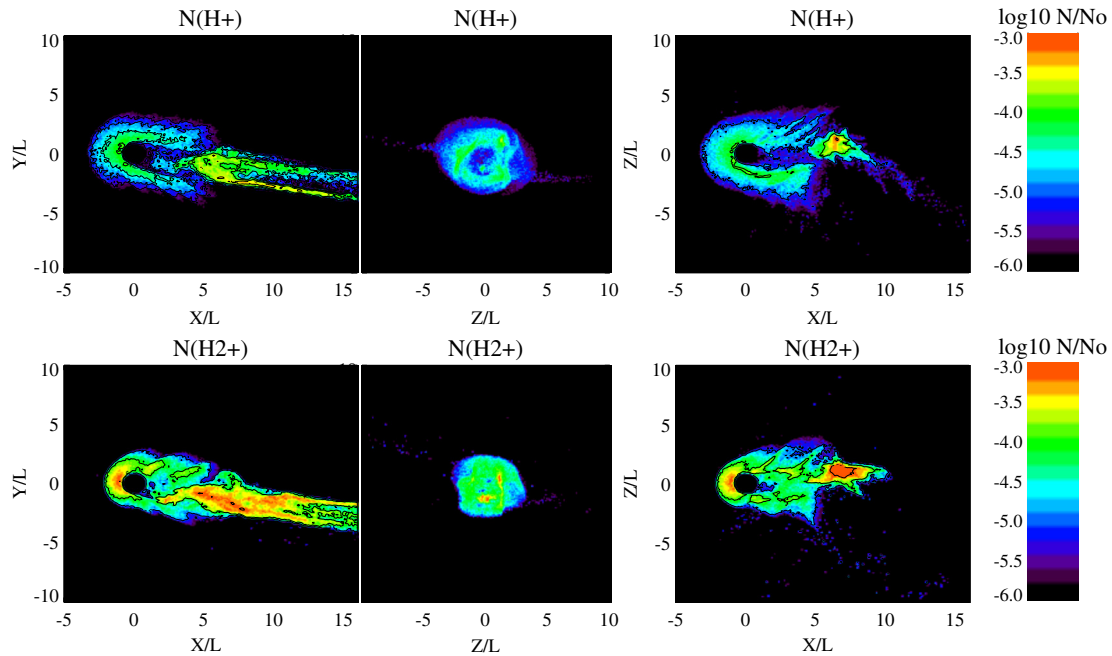


Fig. 2. 2-D cuts of the H^+ , H_2^+ pickup ion (middle and bottom) density profile. Here $No = n_{H^+} = 3.0 \text{ cm}^{-3}$. x - y cuts (left column) are located at $z/L = 0$, y - z cuts (middle column) are located at $x/L = 2.4$, and x - z cuts (right column) are located at $y/L = 0$.

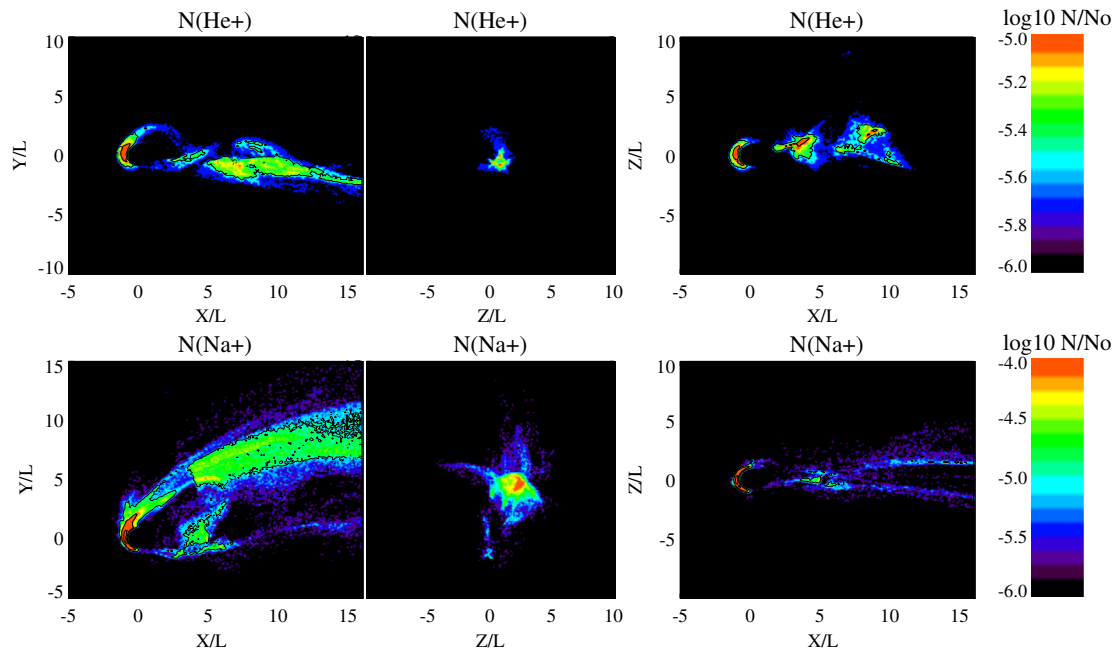


Fig. 3. 2-D cuts of the He^+ , Na^+ pickup ion (middle and bottom) density profile. Here $No = n_{H^+} = 3.0 \text{ cm}^{-3}$. x - y cuts (left column) are located at $z/L = 0$, y - z cuts (middle column) are located at $x/L = 2.4$, and x - z cuts (right column) are located at $y/L = 0$.

Fig. 6 shows the 2-D cuts of the E_y and E_z magnetic field profiles. Here, the x - y cuts (left column) are located at $z/L = 0$, y - z cuts (middle column) are located at $x/L = 2.4$, and x - z cuts (right column) are located at $y/L = 0$. Figs. 4 and 5 (left and right columns, bottom) also confirms a formation of the asymmetrical Mach cone. As one may see that electric field topology follows the upstream H^+ profile for $y < 0$ (asymmetric Mach cone) and weak perturbation in the region of the heavy Na^+

pickup ion mass loading, Fig. 4 (top). The average jumps in the electric field at the front of the Mach cone are about $B_{y,2}/E_0 \approx 1.5$ and $\delta E_x/E_0 \approx 0.5$.

The results of the measurements by the particles and field instruments on the ARTEMIS P1 spacecraft provided new and important information with which realistic model for the plasma interaction can be tested. However, it still needs to be compared the modeling results with observational data in the case when the orbit of satellite is oriented

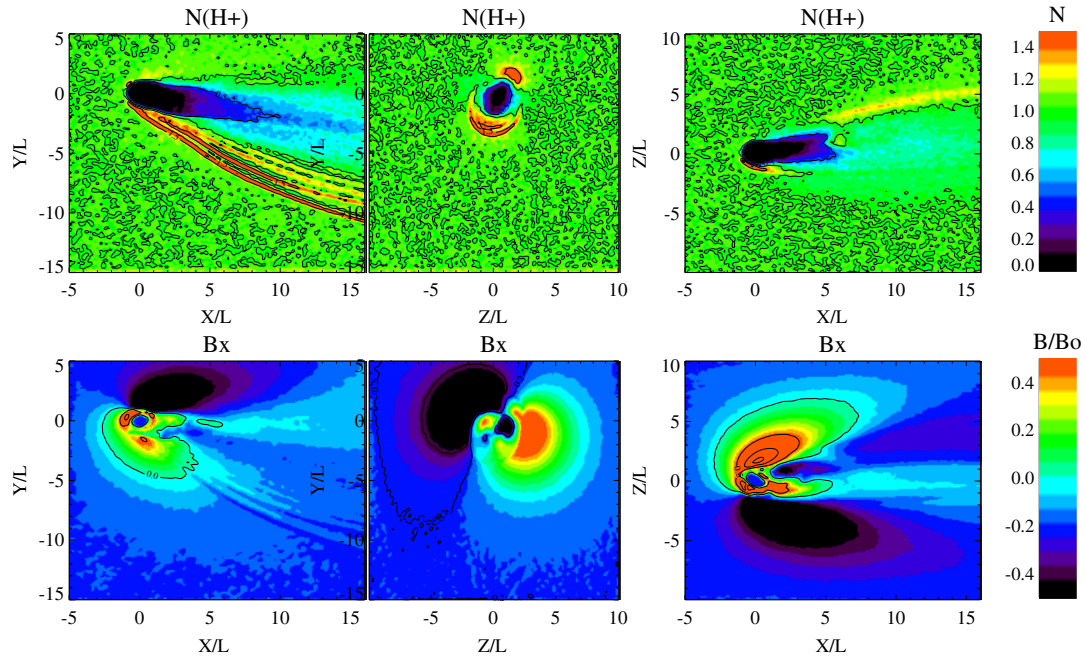


Fig. 4. 2-D cuts of the upstream (background) H^+ ion density (top) and B_x magnetic field B_x (bottom) profile. x - y cuts (left column) are located at $z/L = 0$, y - z cuts (middle column) are located at $x/L = 2.4$, and x - z cuts (right column) are located at $y/L = 0$.

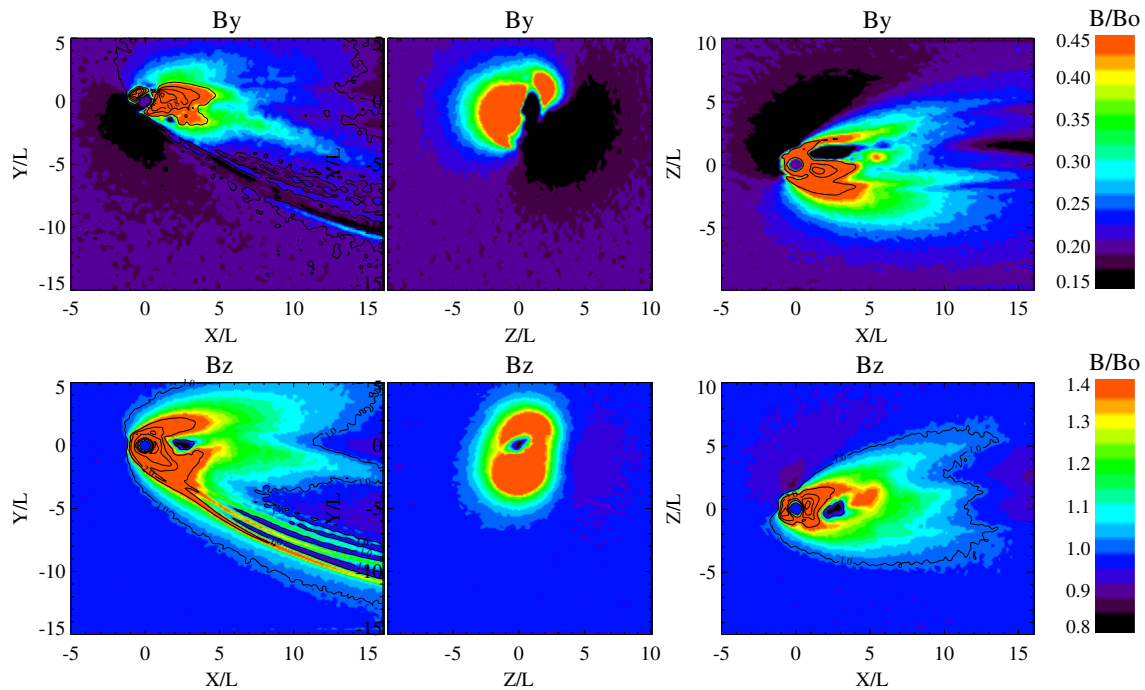


Fig. 5. 2-D cuts of the B_y (top) and B_z (bottom) magnetic field profile. x - y cuts (left column) are located at $z/L = 0$, y - z cuts (middle column) are located at $x/L = 2.4$, and x - z cuts (right column) are located at $y/L = 0$.

perpendicular to the upstream magnetic field. The recent observations (Wang et al., 2011b) indicate the existence of the exospheric H_2^+ ($m/q = 2$) pickup ions. The measurements on board the KAGUYA spacecraft (Tanaka et al., 2009) also observed the Moon-originating ions in the Earth's magnetosphere, so that pickup ion dynamics

become a very important task for interpretation of the recent in-situ investigations of the lunar plasma environment. The results of the modeling of light pickup ions will be discussed in future publications.

Here we have discussed only one model for the lunar exosphere and heavy ion cloud. We should also note that

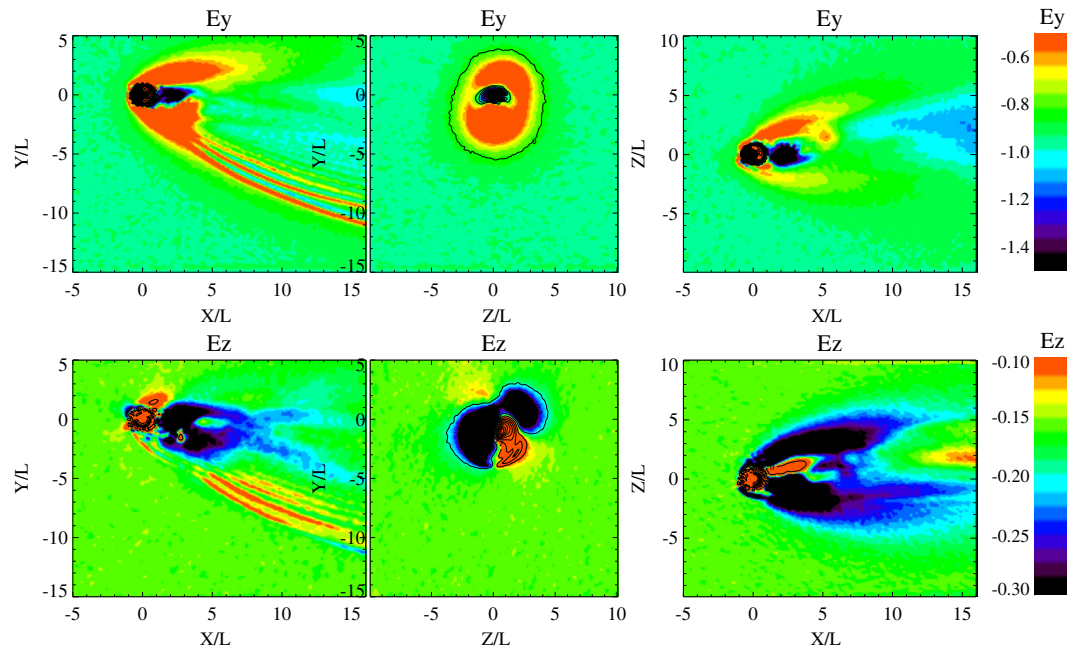


Fig. 6. 2-D cuts of the E_y (top) and E_z (bottom) magnetic field profile. x - y cuts (left column) are located at $z/L = 0$, y - z cuts (middle column) are located at $x/L = 2.4$, and x - z cuts (right column) are located at $y/L = 0$.

the hybrid model for ARTEMIS with heavy ion cloud produces another picture of the plasma-Moon interaction due to solar wind mass loading by the heavy pickup ions.

In the outer region of the exosphere the velocity distributions of the Na^+ , He^+ pickup ions must be ring-like distributions. The ring-type of the velocity distribution for Na^+ , He^+ pickup ions observed in modeling could cause generation of ion cyclotron waves in the far plasma wake. Future modeling possibly will demonstrate the generation of these waves in the distant plasma wake.

One may also see strong phase mixing in the plasma wake. The plasma wake demonstrates the formation of time-dependent structuring in the pickup ion tails and the splitting of the pickup ion tails. Such finite gyroradius effects were also observed in 2.5 D hybrid and bi-fluid modeling of a weak comet and Pluto (see, e.g., Lipatov, 2002; Lipatov et al., 1997; Sauer et al., 1996; Sauer et al., 1997).

Our hybrid modeling shows that the existence of pickup ions near the surface of the Moon may change the global picture of interaction between the solar wind and the Moon due to finite gyroradius effects in compare with the previous studies without the pickup ions (see e.g., Farrell et al., 1998; Birch and Chapman, 2001; Travnicek et al., 2005; Kallio, 2005; Lipatov et al., 2005; Holmström et al., 2012; Wang et al., 2011a; Wiehle et al., 2011). The formation of the asymmetrical Mach cone due to mass loading by pickup ions was also observed in the 2.5 D bi-fluid and 2.5 D/3 D modeling of the weak comet and Pluto (see, e.g., Lipatov, 2002; Lipatov et al., 1997; Sauer et al., 1996; Sauer et al., 1997). In Omidi and Winske (1990), numerical simulations are used to investigate the nonlinear evolution of oblique low-frequency electromagnetic (kinetic magnetosonic) waves, which have been observed

upstream of planetary bow shocks and at comet Giacobini-Zinner. These waves have been referred to as shocklets. In our case we have observed three peaks in the density profile across the Mach cone at a lobe side in the overshoot and downstream. In the y - x plane for $y < 0$ and $x > 5$ we have already observed a strong widening of the three-peak Mach cone structure. The physics of such type Mach code may be different from shocklets formation one since we have no solar wind mass loading for $y < 0$ and it needs further investigation. It will be a subject of future publications.

4. Conclusions

The hybrid modeling of Lunar plasma environment with ARTEMIS parameters with 5 ion species demonstrated several features:

- The light (H^+ , H_2^+ , He^+) and heavy (Na^+) pickup ions form a multiple structured wake with external and internal tails.
- The pickup ions form a conducting layer near the day-side lunar surface and cause a compression in the magnetic field on the day-side of the lunar surface. The mass loading results in the formation of the asymmetrical Mach cone. The split structure of the Mach cone transition produces three peaks in the plasma density, magnetic and electric field distributions.
- The light and heavy pickup ions fill the lunar plasma wake, and, thus, alter the electromagnetic field dynamics in the lunar plasma wake.
- Our modeling may have a capability of broad impact to plasma environment near very weak comets, Pluto, and Europa (Lipatov et al., 1997; Lipatov et al., 2010a; Lipa-

to et al., 2013), and also to solar-wind heat shield interaction, outgassing problem, excitation of the waves in upstream region, plasma wake structure (Lipatov et al., 2010b; Lipatov et al., 2012b).

Currently, we are modeling the heavy (Na^+) and light (He^+ , H_2^+ , H^+) pickup ions dynamics near the Moon in a case with oblique background magnetic field (see e.g. Hartle et al., 2011). We are also modeling the effects of the H^+ and He^+ ions reflected on the day-side of the lunar surface. The result of this modeling will be discussed in future publications. Future modeling must resolve the multiscale effects near the lunar surface, in particular, to provide a realistic distribution of the conductivity inside the lunar interior. These models may include energetic background ions and electrons, and later fully kinetic model including electrons. Future modeling must use the composite grid structure, e.g. “Cubed” sphere grid (Koldoba et al., 2002) to resolve the multiscale effects near the lunar surface and in the outer plasma environment. These approaches will allow us to delete the effects of the reflection of the waves on the side boundaries. This modeling will also allow us to study some kinetic wave-particle interaction effects in the plasma wake, such as the ion cyclotron waves that are expected to be observed in the distant plasma wake.

Acknowledgments

A.S.L., J.F.C., E.C.S., and R.E.H were supported by the Grant *Solar Wind Interaction with Lunar Exosphere and Surface* (PI - J.F. Cooper) from the NASA NRA: Lunar Advance Science and Exploration Research Program (NNH08ZDA001-LASER). A.S.L. was also supported in part by the Grant/task 670-90-315 between the GPHI UMBC and NASA GSFC. Computational resources were provided by the NASA Ames Advanced Supercomputing (NAS) Division (Project SMD-11-2205 and SMP-12-2957). The authors thank the referees for fruitful comments.

References

- Birch, P.C., Chapman, S.C., 2001. Detailed structure and dynamics in particle-in-cell simulations of the lunar wake. *Phys. Plasmas* 8, 4551–4559.
- Braginskii, S.L., 1965. Transport processes in a plasma. In: Leontovich, M.A. (Ed.), *Reviews of Plasma Physics*. Consultants Bureau, New York, pp. 205–240.
- Catto, P.J., 1974. A model for steady interaction of the solar wind with the Moon. *Astrophys. Space Sci.* 26 (10), 47–97.
- Chew, G.F., Goldberger, M.L., Low, F.E., 1956. The Boltzmann equation and the one-fluid hydromagnetic equations in the absence of particle collisions. *Proc. R. Soc. (London)* A236, 112–118.
- Galeev, A.A., Lipatov, A.S., Sagdeev, R.Z., 1987. Two-dimensional numerical simulation of the relaxation of cometary ions and MHD turbulence in the flow of the solar wind around a cometary atmosphere. *Sov. J. Plasma Phys.* 13 (5), 323.
- Gruntman, M., 1996. H_2^+ pickup ions in the solar wind: outgassing of interplanetary dust. *J. Geophys. Res.* 101 (A7), 15555–15568.
- Farrell, W.M., Kaiser, M.L., Steinberg, J.T., Bale, S.D., 1998. A simple simulation of a plasma void: applications to wind observations of the lunar wake. *J. Geophys. Res.* 103 (A10), 23653–23660.
- Halekas, J.S., Angelopoulos, V., Sibeck, D.G., Khurana, K.K., Russell, C.T., Delory, G.T., Farrell, W.M., McFadden, J.P., Bonnell, J.W., Larson, D., Ergun, R.E., Plaschke, F., Glassmeier, K.H., 2011. First results from ARTEMIS, a new two-spacecraft lunar mission: counter-streaming plasma populations in the wake. *Space Sci. Rev.* 165 (1–4), 93–107.
- Hartle, R.E., Killen, R., 2006. Measuring pickup ions to characterize the surfaces and exospheres of planetary bodies: applications to the Moon. *Geophys. Res. Lett.* 33 (L05201), 1–5.
- Hartle, R.E., Sarantos, M., Sittler, E.C., 2011. Pickup ion distributions from three-dimensional neutral exospheres. *J. Geophys. Res.* 116 (A10101), 1–14. <http://dx.doi.org/10.1029/2011JA016859>.
- Hartle, R.E., Thomas, G.E., 1974. Neutral and ion exosphere models for lunar hydrogen and helium. *J. Geophys. Res.* 79 (10), 1519–1526.
- Holmström, M., Fatemi, S., Futaana, Y., Nilsson, H., 2012. The interaction between the Moon and the solar wind. *Earth Planets Space* 64 (2), 237–245.
- Kallio, E., 2005. Formation of the lunar wake in quasi-neutral hybrid model. *Geophys. Res. Lett.* 32 (L06107), 1–5.
- Koldoba, A.V., Romanova, M.M., Ustyugova, G.V., Lovelace, R.V.E., 2002. Three dimensional MHD simulation of accretion to an inclined rotator: The cubed sphere method. *Astrophys. J.* 576 (1), L53–L56. <http://dx.doi.org/10.1086/342780>.
- Lee, D.-W., Kim, S.J., Lee, D.H., Jin, H., Kim, K.S., 2011. Three-dimensional simulation of the lunar sodium exosphere and its tail. *J. Geophys. Res.* 116 (A07213). <http://dx.doi.org/10.1029/2011JA016451>.
- Lipatov, A.S., 1974. The guiding center in a cell method in the three-dimensional problem on the interaction of the solar wind plasma with the conducting model of the moon (Numerical experiment), Moscow, Academy of Sciences USSR, Institute of Space Research, Report Pr-196, pp. 1–39 (in Russian).
- Lipatov, A.S., 1975. The guiding center in a cell method in the three-dimensional problem on the interaction of the solar wind plasma with the conducting model of the Moon (Numerical experiment), NASA Technical Translation, NASA TT F-16, vol. 414. Washington, D.C.
- Lipatov, A.S., 1976. About three-dimensional structure of the lunar wake. *Cosmic Res. (Sov. J. Kosmich. Issled)* 14 (1), 103–106.
- Lipatov, A.S., 2002. *The Hybrid Multiscale Simulation Technology: An Introduction With Application To Astrophysical and Laboratory Plasmas*. Springer-Verlag, Berlin, Heidelberg, New York (pp. 1–403).
- Lipatov, A.S., 2012. Merging for particle-mesh complex particle kinetic modeling of the multiple plasma beams. *J. Comput. Phys.* 231, 3101–3118.
- Lipatov, A.S., Combi, M.R., 2006. Effects of kinetic processes in shaping Io's global plasma environment: a 3D hybrid model. *ICARUS* 180 (2), 412–427.
- Lipatov, A.S., Cooper, J.F., 2010. Hybrid kinetic modeling of the Lunar plasma environment: past, present and future. In: *Lunar Dust, Plasma and Atmosphere: The Next Steps*, January 27–29, Boulder, Colorado, Abstracts/lpa2010.colorado.edu/.
- Lipatov, A.S., Cooper, J.F., Paterson, W.R., Sittler, E.C., Hartle, R.E., Simpson, D.G., 2010a. Jovian plasma torus interaction with Europa: 3D hybrid kinetic simulation. *First Results Planet. Space Sci.* 58, 1681–1691.
- Lipatov, A.S., Cooper, J.F., Sittler, E.C., Hartle, R.E., 2011. Effects of pickup ions on the solar wind near the lunar-like objects: 3D hybrid modeling. In: *Proceeding of the Extended Abstracts, European Planetary Science Congress-DPS Joint Meeting 2011*, October 2–7, 2011, Nantes, France, Session TP/MG8/SB14, vol. 6, Paper EPSC-PDS2011-95.
- Lipatov, A.S., Cooper, J.F., Sittler, E.C., Hartle, R.E., 2012a. Effects of Na^+ and He^+ pickup ions on the lunar-like plasma environment: 3D hybrid modeling. *Adv. Space Res.* 50, 1583–1591.

- Lipatov, A.S., Cooper, J.F., Paterson, W.R., Sittler Jr., E.C., Hartle, R.E., Simpson, D.G., 2013. Jovian plasma torus interaction with Europa. Plasma wake structure and effect of inductive magnetic field: 3D hybrid kinetic simulation. *Planet. Space Sci.* 77, 12–24.
- Lipatov, A.S., Motschmann, U., Bagdonat, T., 2002b. 3-D hybrid simulation of the interaction of the solar wind with a weak comet. *Planet. Space Sci.* 50, 403–411.
- Lipatov, A.S., Motschmann, U., Bagdonat, T., Griessmeier, J.-M., 2005. The interaction of the stellar wind with an extrasolar planet – 3D hybrid and drift-kinetic simulations. *Planet. Space Sci.* 53, 423–432.
- Lipatov, A.S., Sauer, K., Baumgärtel, K., 1997. 2.5-D hybrid code simulation of the solar wind interaction with weak comets and related objects. *Adv. Space Res.* 20 (2), 279–282.
- Lipatov, A.S., Sittler Jr., E.C., Hartle, R.E., Cooper, J.F., 2010. The interaction of the solar wind with solar probe plus – 3D hybrid simulation. Report 2: The study for the distance 9.5 Rs. Technical, Memorandum NASA/TM-2010-215863, December, pp. 1–117.
- Lipatov, A.S., Sittler Jr., Hartle, R.E., Cooper, J.F., 2012b. Short wavelength electromagnetic perturbations excited near the solar probe plus spacecraft in the inner heliosphere: 2.5D hybrid modeling. *Planet. Space Sci.* 62, 61–68.
- Lipatov, A.S., Zank, G.P., Pauls, H.L., 1998. The interaction of neutral interstellar H with the heliosphere: a 2.5-D particle-mesh boltzmann simulation. *J. Geophys. Res.* 103 (A9), 20631–20642.
- McLain, J.L., Sprague, A.L., Grieves, G.A., Schriver, D., Travnicek, P., Orlando, T.M., 2011. Electron-stimulated desorption of silicates: a potential source for ions in Mercury's space environment. *J. Geophys. Res.* 116 (E03007), 1–9. <http://dx.doi.org/10.1029/2010JE003714>.
- Omidi, N., Winske, D., 1990. Steepening of kinetic magnetosonic waves into shocklets: simulations and consequences for planetary shocks and comets. *J. Geophys. Res.* 95 (A3), 2281–2300.
- Potter, A.E., Morgan, T.H., 1988. Discovery of sodium and potassium vapor in the atmosphere of the Moon. *Science* 241, 675–680. <http://dx.doi.org/10.1126/science.241.4866.675>.
- Sauer, K., Bogdanov, A., Baumgärtel, K., Dubinin, E., 1996. Plasma environment of comet Wirtanen during its low-activity stage. *Planet. Space Sci.* 44 (7), 715–729.
- Sauer, K., Lipatov, A.S., Baumgärtel, K., Dubinin, E., 1997. Solar wind-pluto interaction revised. *Adv. Space Res.* 20 (2), 295–299.
- Spreiter, J.R., Marsh, M.C., Summers, A.L., 1970. Hydrodynamic aspects of solar wind flow past the Moon. *Cosmic Electrodynamics* 1, 5–50.
- Tanaka, T., Saito, Y., Yokota, S., Asamura, K., Nishino, M.N., Tsunakawa, H., Shibuya, H., Matsushima, K., Shimizu, H., Takahashi, F., Fijimoto, M., Mukai, T., 2009. First in situ observation of the Moon-originating ions in the Earth's magnetosphere by MAP-PACE on SELENE (KAGUYA). *Geophys. Res. Lett.* 36 (L22106), 1–5. <http://dx.doi.org/10.1029/2009GL040682>.
- Tao, J.B., Ergun, R.E., Newman, D.L., Halekas, J.S., Anderson, L., Angelopoulos, V., Bonnell, J.W., McFadden, J.P., Cully, C.M., Auster, H.-U., Glassmeier, K.-H., Larson, D.E., Baumjohann, W., Goldman, M.V., 2012. Kinetic instabilities in the lunar wake: ARTEMIS observations. *J. Geophys. Res.* 117 (A03106). <http://dx.doi.org/10.1029/2011JA017364>.
- Travnicek, P., Hellinger, P., Schriver, D., Bale, S.D., 2005. Structure of the lunar wake: two-dimensional global hybrid simulations. *Geophys. Res. Lett.* 32 (L06102), 1–4. <http://dx.doi.org/10.1029/2004GL022243>.
- Tyler, A.L., Kozlowski, R.W.H., Hunten, D.M., 1988. Observations of sodium in the tenuous lunar atmosphere. *Geophys. Res. Lett.* 15 (10), 1141–1144. <http://dx.doi.org/10.1029/GL015i010p01141>.
- Whang, Y.C., 1969. Field and plasma in the Lunar wake. *Phys. Rev.* 186 (1), 143–150.
- Whang, Y.C., Ness, N.F., 1970. Observation and interpretation of the lunar Mach cone. *J. Geophys. Res.* 75 (31), 6002–6010.
- Wang, Y.-C., Müller, J., Ip, W.-H., Motschmann, U., 2011a. A 3D hybrid simulation study of the electromagnetic field distributions in the lunar wake. *Icarus* 216, 415–425.
- Wang, X.-D., Zong, Q.-G., Wang, J.-S., Cui, J., Réme, H., Dandouras, I., Aoustin, C., Tan, X., Shen, J., Ren, X., Liu, J.-J., Zuo, W., Su, Y., Wen, W.-B., Wang, F., Fu, Q., Mu, L.-L., Wang, X.-Q., Geng, L., Zhang, Z.-B., Liu, J.-Z., Zhang, H.-B., Li, C.-L., Quyang, Z.-Y., 2011b. Detection of $m/q = 2$ pickup ions in the plasma environment of the Moon: the trace of exospheric H_2^+ . *Geophys. Res. Lett.* 38 (L14204), 1–5. <http://dx.doi.org/10.1029/2011GL047488>.
- Wiehle, S., Plaschke, F., Motschmann, U., Glassmeier, K.-H., Auster, H.U., Angelopoulos, V., Mueller, J., Krieger, H., Georgescu, E., Halekas, J., Sibeck, D.G., McFadden, J.P., 2011. First lunar wake passage of artemis: discrimination of wake effects and solar wind fluctuations by 3D hybrid simulations. *Planet. Space Sci.* 59 (8), 661–671.
- Winske, D., Wu, C.S., Li, Y.Y., Mou, Z.Z., Guo, S.Y., 1985. Coupling of newborn ions to the solar wind by electromagnetic instabilities and their interaction with the bow shock. *J. Geophys. Res.* 90, 2713–2726.
- Wolf, R.A., 1968. Solar-wind flow behind the Moon. *J. Geophys. Res.* 73 (13), 4281–4289.
- Wurz, P., Rohner, U., Whitby, J.A., Kolb, C., Lammer, H., Dobnikar, P., Martín-Fernández, J.A., 2007. The lunar exosphere: the sputtering contribution. *Icarus* 191, 486–496.